



Supplementary Materials for

Multiplex recording of cellular events over time on CRISPR biological tape

Ravi U. Sheth, Sung Sun Yim, Felix L. Wu, Harris H. Wang*

*Corresponding author. Email: hw2429@columbia.edu

Published 23 November 2017 on *Science* First Release
DOI: 10.1126/science.aao0958

This PDF file includes:

Materials and Methods
Figs. S1 to S16
Tables S1 to S5
References

Materials and Methods

Plasmid construction

All plasmids (table S1) were constructed via the Golden Gate method (31) with the NEB 10-beta cloning strain (NEB, C3019H) and were verified via Sanger sequencing (Eton Bioscience, Genewiz). All plasmids are deposited at Addgene. The RBS calculator (32) and Anderson library of promoters (<http://parts.igem.org/Promoters/Catalog/Anderson>) were utilized as annotated on plasmid maps.

The pTrig plasmid was generated from pSB2K3-BBa_J04450 (iGEM 2016 distribution), which itself was derived from the pSCANS vector (<http://genome.bnl.gov/Vectors/pscans.php>). To construct pTrig, the BBa_J04450 (RFP) sequence and Biobrick multiple cloning site were removed; the resulting plasmid contains the mini-F origin and replication machinery, P1 lytic replication element RepL placed downstream of an IPTG-inducible Lac promoter, and kanamycin resistance marker.

The pRec plasmid was generated by placing the *E. coli cas1-cas2* cassette (amplified from NEB 10-beta) downstream of the $P_{LTetO-1}$ promoter (33) on a ColE1 plasmid containing chloramphenicol resistance marker and constitutively expressed TetR and LacI (LacI is required to repress the Lac promoter on pTrig, see fig. S1).

For the CopA sensor, a derivative of the pTrig plasmid (pTrig-CopA) containing the *E. coli* BL21 CopA promoter (100 bp upstream sequence) with RiboJ (34) and B0034 RBS was constructed. This was utilized with a derivative of the pRec plasmid without LacI (pRec Δ LacI).

For the GalS and TreR sensors, derivatives of the pRec plasmid containing LacI chimeric transcription factors (pRec-TreR, pRec-GalS) were constructed by swapping the LacI ligand binding domain with either the TreR or GalS ligand binding domains and then subsequently introducing point mutations that have been characterized to improve sensor performance (TreR: V52A; GalS: Q54A, E232K) (35). These pRec variants were then utilized with the pTrig plasmid.

Chromosomal alteration of strains with MAGE

Given that we utilized LacI chimeric transcription factors (GalS, TreR) we generated a variant of the *E. coli* BL21 strain lacking endogenous expression of LacI to prevent interaction with the sensing systems. We utilized the MODEST tool to design a recombineering primer (MAGE_tKO_lacI, table S3) to perform a translational knockout of chromosomal LacI by introduction of three stop codons into the beginning of the *lacI* coding sequence (36). Briefly, the BL21 strain was transformed with pKD46 (37) and grown at 30 °C with 50 μ g/mL Carbenicillin (Fisher BP2648). An overnight culture of this strain was back-diluted and grown for 30 min, 0.5% arabinose was added, and the culture was grown to approximately OD600 = 0.6. 1 mL of cells were then placed on ice and washed with nuclease-free water 3 times, resuspended in 2.5 μ M oligonucleotide at a volume of 50 μ L, and subjected to electroporation. Cells were then recovered for 1 hour at

30 °C. This process constituted one round of recombineering; after this procedure cells were plated on LB-agar with antibiotics and X-gal (200 µg/mL, Thermo FERR0404) and grown at 30 °C. Resulting clones were screened for loss of LacI expression by beta-galactosidase assay (loss of LacI expression de-represses LacZ), and a resulting clone was verified to contain the correct chromosomal alteration by Sanger sequencing. This strain was hereafter denoted BL21 LacI_tKO.

Oligo recombineering was also utilized to introduce barcodes into the genomic CRISPR array first direct repeat (DR) sequence. A recombineering primer (MAGE_BL21_DR, table S3) was designed to mutagenize the distal 7 bp of the DR sequence (inadvertently, we also targeted the first base pair of the first native genomic spacer for mutagenesis, resulting in 8 bp total targeted for mutagenesis). The BL21 LacI_tKO strain, still harboring pKD46 was subjected to five rounds of oligo recombineering as described above. The resulting cell population was then subjected to heatshock at 42 °C for 1 hour to promote loss of pKD46 and recovered overnight at 37 °C in LB without antibiotics; a cryostock of the population (15% glycerol) was saved for subsequent screening for clones with barcoded DR sequences.

Experimental conditions (induction of pRec and pTrig)

All testing was conducted in *E. coli* BL21 (NEB C2530H), a strain that contains two genomic CRISPR arrays but lacks *cas* interference machinery (38). For induction experiments with the LacI sensor, the *E. coli* BL21 strain was transformed with appropriate plasmids (pRec, or pRec+pTrig) via electroporation (table S2). A single colony was picked and grown to stationary phase and a cryostock (15% glycerol) was created for storage at -80 °C.

The general experimental workflow of an induction experiment was as follows:

1. A culture tube (Thomas Scientific 110158PL-TS) containing 3 mL autoclaved LB-Lennox (BD 240230) and appropriate antibiotics at indicated final concentrations (pRec: chloramphenicol 34 µg/mL [EMD Millipore Omnipur 3130, diluted in 100% ethanol], pTrig: kanamycin 50 µg/mL [Fisher BP906-5, diluted in nuclease free water]) was inoculated from the culture glycerol stock and grown overnight (>12 hours) at 37 °C in an Innova44 incubator shaker at 230 rpm.
2. The next day, this culture was diluted 1:100 into a new tube containing 3 mL LB media and appropriate antibiotics and allowed to grow in the same culture conditions for 2 hours to bring cultures into exponential phase.
3. This culture was then diluted 1:100 into a new tube containing 3 mL LB media, appropriate antibiotics, and appropriate anhydrotetracycline (aTc) and isopropyl β-D-1-thiogalactopyranoside (IPTG) inducers at indicated final concentrations (aTc: 100 ng/mL [Cayman 10009542, diluted in 100% ethanol], IPTG: 1 mM [Thermo R0392, diluted in nuclease free water]). This culture was then allowed to grow in the same culture conditions for 6 hours.

4. Finally, culture from this tube was diluted 1:100 into a new tube containing 3 mL LB media and appropriate antibiotics, and allowed to recover in the same culture conditions overnight for 16 hours.
5. At the conclusion of the experiment 500 μ L of culture was transferred to a 1.5 mL tube (VWR 20170-333), the tube was spun down (15,000 rpm, 30s) to pellet cells, media was removed, and the pellet was stored at -20°C for subsequent analysis.

Experimental conditions (temporal recordings)

For 4 day temporal recording experiments the induction procedure as above was utilized, but after the first day, recovery cultures from the previous day were diluted. starting at step 2 of protocol. All cultures were exposed to aTc and received no IPTG or 1mM IPTG. Samples were collected from each recovery culture for analysis. As noted, the experiment was performed in a branched manner, in that a single culture from a previous day was used to inoculate two daughter cultures (one receiving IPTG inducer, one not).

For the 10 day temporal recording experiment, 8 exposure profiles were randomly generated and conducted in a similar manner over the course of 10 days (1010001010, 1001011001, 1001010101, 0111111001, 0101011010, 0100110110, 0100101010, 0001100010; 1 indicates induction and 0 indicates no induction) and samples were collected from d4 to d10. The experiment was also performed in a branching manner as above; therefore given that the starting substring of some samples were shared, some shorter time points had less than 8 samples (d4-d5:6, d6:7, d7-d10:8).

Experimental conditions (multiplexed recording)

To generate barcoded strains with the three additional sensors for the multiplexed recording experiment, 100 μ L of the BL21 LacI_tKO with mutagenized DR cryostock was re-inoculated into an overnight culture of LB with no antibiotics. The appropriate pRec and pTrig plasmids for the TreR and GalS sensors (table S2) were transformed into this population via electroporation. Colonies were then picked and screened for mutated DR sequence via Sanger sequencing. This yielded mutated DR sequences for TreR (ATGGGTCC, underline denotes altered sequence from WT) and GalS (ACATCAG). We note that the GalS strain also contained a mutation in the first basepair of the first native genomic spacer (G to A) due to inadvertent targeting; however, this did not affect analysis given thresholds utilized in matching during sequencing analysis. The TreR background strain is referred to as BL21 LacI_tKO DR_mut_1 and the GalS background strain BL21 LacI_tKO DR_mut_2. The plasmids for the CopA sensor (table S2) were separately transformed into *E. coli* BL21. The three sensor strains were then grown separately in filter sterilized M9 media with appropriate antibiotics (1X M9 salts [BD 248510], 0.8% (wt/vol) glycerol [Fisher G33-1], 0.2% (wt/vol) casamino acids [BD 223120], 2 mM MgSO₄ [Sigma-Aldrich 230391], 0.1 mM CaCl₂ [Sigma-Aldrich C1016]) and a cryostock (15% glycerol) was created for storage at -80°C .

The general experimental workflow followed the temporal recording induction protocol with minor modification. All multiplexed recordings were conducted in M9 media. The three strains were grown overnight separately, optical density was measured, and the three

strains were pooled at equal densities. The initial dilution (step 2) was 1:10 rather than 1:100 given slower growth rate in M9 media compared to LB. Before recovery (step 4), cells were spun down (15,000 rpm, 30s), media was removed and cells were resuspended in 1mL of fresh media to remove any residual inducer. Inducers for the three sensors were as follows, CopA: 100 μ M copper sulfate (Sigma-Aldrich 209198), TreR: 1 mM trehalose (Sigma-Aldrich T9531), GalS: 1 mM fucose (Sigma-Aldrich F8150).

qPCR assay for pTrig copy number

A qPCR plasmid copy number assay was utilized to assay pTrig copy number. Briefly, 18 μ L of a qPCR master mix (10 μ L 2X KAPA SYBR Fast qPCR Master Mix [KAPA KK4601], 0.6 μ L 10 μ M forward primer, 0.6 μ L 10 μ M reverse primer, 6.8 μ L nuclease free water) was dispensed into a 96 well qPCR plate (Bio-Rad HSL9905) and 2 μ L of template as prepared during sequencing library preparation (see protocol below) was added. Two qPCRs were performed, the first with primers targeting pTrig and the second with primers targeting the genome (derived from (39), see table S3 for sequences). Both primer pairs were confirmed to have >90% amplification efficiency. The PCR plates were sealed with optically transparent film (Bio-Rad MSB1001) and were placed on a qPCR system (Bio-Rad CFX96) and subjected to following cycling conditions: 95 °C 3 min, 39 cycles: 95 °C 3 s, 60 °C 20 s, 72 °C 1 s and acquisition. The Cq values were determined via the manufacturer's software, and pTrig relative enrichment was calculated with the delta delta Cq method (i.e. $2^{(-1*(pTrig_Cq - 16S_Cq))}$), normalized to the lowest value). A melt curve was performed to ensure that only a single amplification product was present.

Design of custom CRISPR array sequencing scheme

Our custom sequencing scheme enabled highly efficient use of Illumina read lengths (up to 5 expanded spacers with a 300 cycle sequencing kit) by avoiding re-sequencing of primer sequences as required with most two-step amplification schemes. To design these primers for CRISPR BL21 sequencing (referred to as "CB"), we utilized a forward primer targeting the BL21 array I leader sequence and a reverse primer targeting the array I first native genomic spacer. The forward primer was linked to an Illumina P5 sequence and barcode sequence; we generated a series of 8 (i.e. CB501-CB508). The reverse primer was linked to an Illumina P7 sequence and barcode sequence; we generated a series of 12 (i.e. CB701-CB712). All barcode sequences were derived from Illumina Nextera indices. The combination of 8x12 primers allows for 96 samples to be uniquely barcoded via dual indexing in a single sequencing run. We generated custom read 1 (CBR1) and index 1 (CBI1) sequencing primers. All primer sequences can be found in table S4. All primers in this study were obtained from IDT with normal desalting purification.

CRISPR array sequencing library preparation protocol

To perform sequencing of CRISPR arrays from populations of cells, we developed a library preparation and sequencing pipeline consisting of three steps: (1) gDNA preparation, (2) PCR amplification and (3) sample pooling, purification, and quality control.

To purify gDNA from cell pellets obtained at the end of an experiment, we developed a modified protocol utilizing the prepGEM Bacteria kit (ZyGEM PBA0500; VWR 95044-082). Cell pellets were removed from storage at -20°C in 1.5 mL tubes and resuspended in 100 μL of TE (10 mM Tris-HCl pH 8.0 [Fisher BP1758], 1 mM EDTA pH 8.0 [Sigma-Aldrich 03690] in nuclease free water [Ambion AM9937]). 10 μL of the resulting suspension was pipetted into a 96-well skirted PCR plate (Eppendorf 951020401). 20 μL of a prepGEM master mix (0.30 μL prepGEM enzyme; 0.30 μL lysozyme enzyme, 3.0 μL 10X Green Buffer, 16.4 μL nuclease free water) was then added to each well with a multichannel pipette, and the plate was heat sealed (Vitr V901004 and Vitr V902001). The plate was then spun down for 30 seconds on a plate microfuge (Axygen C1000-AXY) and incubated on a PCR thermocycler (Bio-Rad S1000) with the following program: 37°C 15 min, 75°C 15 min, 95°C 15 min, 4°C infinite. 70 μL of TW (10 mM Tris-HCl pH 8.0 in nuclease free water) was then added to each well with a multichannel pipette.

To prepare uniquely barcoded amplicons for each sample, we performed PCR amplification using the CB50X and CB7XX sequencing primers (table S4). First, a master primer-plate was prepared by arraying the CB50X primers across rows of a 96-well PCR plate and CB7XX primers down columns of the same 96-well PCR plate at a final concentration of 10 μM for each primer in 50 μL . Thus, each well contained a unique combination of CB50X and CB7XX primers. A PCR reaction was then set up for each sample by pipetting 2 μL of the mix from the master primer-plate, 5 μL of gDNA from prepared genomic DNA plate and 13 μL of a PCR master-mix (10 μL NEB Next Q5 Hot Start HiFi PCR Master Mix [NEB M0543L], 2.96 μL nuclease free water, 0.04 μL SYBR Green I 100X [1:100 dilution in nuclease free water of 10,000X SYBR Green I concentrate, ThermoFisher S7567]) into a new 96-well PCR plate. Alongside each set of samples, a no template control (NTC) was performed as a quality control measure utilizing nuclease-free water rather than gDNA as template. The plate was sealed with optically transparent film (Bio-Rad MSB1001), spun down for 30 seconds on a plate microfuge, placed on a qPCR system (Bio-Rad CFX96), and the following PCR program was performed: 98°C 30 s, 29 cycles: 98°C 10 s, 65°C 75 s, 65°C 5 min, 4°C infinite. Amplification was observed and stopped while samples remained in exponential amplification (typically 12-15 cycles).

To perform pooling and quality control of the resulting sample amplicons, representative samples and the NTC were assessed on a 2% E-Gel (ThermoFisher G402002 and G6465) for presence of the expected product (164 bp unexpanded CRISPR array product, and expanded products; each new spacer expansion results in addition of ~ 61 bp) and no observable product in the NTC. Next, a SYBR Green I plate assay was performed to quantify the relative concentration of amplicon present in each PCR product. Concentrated 10,000X SYBR Green I stock was diluted to a final concentration of 1X in TE, and 198 μL was pipetted with a multichannel pipette into wells of a black optically transparent 96 well plate (ThermoFisher 165305). 2 μL of PCR product was added to each well, and the plate was allowed to incubate in a dark location for 10 minutes. Fluorescence of each well (excitation: 485 nm, emission: 535 nm) was measured on a microplate reader (Tecan Infinite F200), and fluorescence values for individual samples were background subtracted with the fluorescence value of the NTC to control for presence of primers in each PCR. Using this background subtracted fluorescence value, samples were pooled using a Biomek

4000 robot such that equal arbitrary fluorescence units of each sample were present in the final pool.

To remove primers from the pooled product in a manner that did not affect abundance of different amplicon products, the pool was then subjected to gel electrophoresis (2% agarose gel, 100 V) and gel extracted (Promega A9282) from size ranges ~150 bp to ~1 kb, and eluted in 30 μ L TW in an LoBind tube (Eppendorf 022431021). The amount of DNA present in purified pool was quantified (Qubit dsDNA HS Assay Kit, ThermoFisher Q32854 with Qubit 3.0 Fluorometer, ThermoFisher Q33216) with at least two replicates performed with different pipettes and the average fragment size was quantified on an Agilent Bioanalyzer 2100 with Bioanalyzer High Sensitivity DNA kit (Agilent 5067-4626). The molar concentration of the pool was determined with use of Qubit fluorometric quantification and Bioanalyzer size determination.

Size-enrichment of CRISPR array libraries

For selected libraries, a size-enrichment protocol was performed to enrich for expanded arrays and deplete unexpanded arrays. We utilized SPRI bead-based size selection with AMPureXP beads (Beckman Coulter A63881); altering the ratio of AMPureXP added to a particular sample can allow for size selection of a particular library. Rather than performing gel extraction as in the normal library preparation protocol, pooled PCR products were subject to two AmpureXP cleanups with 0.75X ratio of AmpureXP beads to volume of PCR product. These cleanups were performed as per the manufacturer's recommendations with minor modifications: 80% ethanol rather than 70% ethanol, elution into 33 μ L TW and removal of 30 μ L (to reduce carryover of beads).

We found that the resulting libraries displayed enrichment of larger DNA products which did not appear to be CRISPR arrays and were presumably plasmid or degraded genomic DNA carrying through from the template. This did not alter quality of the resulting library, but to better assess concentration of the library, a qPCR quantification (NEB E7630L) was utilized in addition to fluorometric quantification.

Sequencing CRISPR array libraries

Sequencing was performed on the Illumina MiSeq platform (reagent kits: V3 150 cycle, V2 300 cycle, Micro V2 300 cycle depending on the experiment). All runs included at least a 20% PhiX spike-in (PhiX Sequencing Control V3) which was necessary for run completion given relatively low sequence diversity and variable amplicon size. For V3 kits, samples were loaded at 15 pM final concentration, while for V2 kits samples were loaded at 10-12 pM final concentration following the manufacturer's instructions with the following modifications. First, to spike in custom sequencing primers, 6 μ L of a 100 μ M stock of the CBR1 primer (table S4) was spiked into well 12 of the reagent cartridge utilizing an extended length tip (Rainin RT-L200XF). Similarly, 6 μ L of a 100 μ M stock of the CBI1 primer (table S4) was spiked into well 13 of the reagent cartridge. This spike-in procedure was necessary (rather than utilizing custom primer wells) to allow for the PhiX control to be sequenced with primers already present in the standard primer wells (40). Second, we note that significant amounts of sample may be retained in the sample

loading line from run to run (*Illumina Technical Support Note: Reducing Run-to-Run Carryover on the MiSeq Using Dilute Sodium Hypochlorite Solution*), which may result in contamination of samples indexed with similar barcodes. Therefore, after every run we performed an optional template line wash, and where possible utilized unique barcodes for adjacent runs.

CRISPR spacer extraction and mapping from sequencing data

Raw sequencing reads were analyzed with a custom Python analysis pipeline. Code utilized for sequencing analysis can be found at <https://github.com/ravisheth/trace>. Briefly, the pipeline comprised the following steps: (1) raw reads were subjected to spacer extraction, (2) extracted spacers were then mapped against genome and plasmid references to determine their origin, (3) uniquely mapping spacers were determined from mapping results.

To extract spacers (*spacer_extraction.py*), we began with raw reads (given the low error rates of the Illumina platform, and highly structured nature of sequences, we found filtering of raw sequences to be unnecessary). For each read, we checked the beginning 12 bp of the read to ensure that this matched the expected DR sequence. If this criterion was passed, the DR sequence was stripped from the 5' of read and the remaining sequence was passed into a spacer extraction loop. First, the 5' of the remaining read sequence was compared to the native genomic first spacer sequence (i.e. end of potential newly acquired spacers); if a match was found we considered the read terminated and recorded any spacers extracted, or that the array was unexpanded if no spacers were extracted. If the sequence did not match, we attempted to find a DR sequence given different possible spacer lengths, in this case 32-34 bp (19). If a DR sequence was identified, the spacer was extracted, the spacer and DR sequence were stripped from the 5' of the read, and the extraction loop was repeated for the remaining sequence. For sequencing runs with 150-159 bp read length, we utilized the full DR sequence during matching, which enabled extraction of up to two new spacers. However, for sequencing runs with 309 bp read length (i.e. maximum possible with 300 cycle reagent kit), only 15 bp of the 5' of the DR sequence was utilized for matching given read length constraints (using full length DR sequences would only allow for extraction of 4 new spacers). For all multiplexed temporal recordings, the full length DR sequence was utilized to enable differentiation of DR sequences. This extraction routine allowed for high efficiency read extraction (for example, on average >97% of all reads could be extracted without error for each sample).

To map spacers against reference (*blast_search.sh*), the extracted spacers were searched against reference databases of the genome (NCBI GenBank CP001509.3) and plasmids (as appropriate given the sample) using NCBI BLAST 2.6.0 (41). Extracted spacer files generated by the extraction pipeline were passed to the *blastn* command, using the flag *-evalue 0.0001* to threshold spurious mapping results (21).

Finally, the resulting BLAST output files were analyzed and spacers mapping to only one reference were determined (*unique_spacers.py*). This was necessary given that the plasmids may share sequence homology with the reference genome. The resulting uniquely mapping spacers were saved to an output file for further analysis. For analysis of array

types frequencies, only arrays with all spacers uniquely mapping to one reference were analyzed.

Model of CRISPR array expansion and reconstruction of temporal input profiles

We utilized a simple model of CRISPR expansion. We consider a population of CRISPR arrays that undergoes an expansion process during each round of induction. The parameters governing the expansion process are dependent on the identity of the round (if pTrig is activated or not). Specifically:

- Each array can undergo expansion with probability p_{exp} . The acquired spacer can be:
 - A trigger spacer with probability p_T
 - A reference spacer with probability $p_R = 1 - p_T$
- The probability of an array not undergoing expansion is $1 - p_{exp}$

Therefore, for each state (0: no pTrig activation; 1: pTrig activation), two parameters govern the expansion process (p_{exp}, p_T) for a total of four parameters ($p_{exp,0}, p_{T,0}, p_{exp,1}, p_{T,1}$) governing the entire model. To determine these parameters, we utilized control experiments as well as the “1111” and “0000” samples; all model parameters can be found in table S5. To calculate $p_{exp,0}$ and $p_{exp,1}$, the average proportion of singly expanded arrays after a single round of induction (with and without pTrig activation) was determined from control experiments. To calculate $p_{T,0}$, we used the average pTrig incorporation rate across all array lengths and positions (L1 to L5, p1 to p5) from the “0000” sample. To calculate $p_{T,1}$, we similarly utilized pTrig incorporation frequencies from the “1111” sample. However, the pTrig incorporation rate appeared to decrease with array length; this is likely due to the fact that CRISPR expansion precedes full pTrig activation in our experimental scheme, resulting in highly expanded arrays containing a lower proportion of pTrig spacers (fig. S9). To account for these differences, we parameterized an “apparent pTrig incorporation rate” for different array lengths based on the “1111” sample by calculating the average pTrig incorporation at each array length. When simulating expected array-type frequencies for different array lengths, the corresponding $p_{T,1}$ for that array length was utilized (i.e. $p_{T,1}^{L1}$ to $p_{T,1}^{L5}$).

We then calculated predicted array-type frequencies given a particular temporal input profile and parameterized model. Specifically, all possible array-types were enumerated for a given array-length. We calculated the probability of generating each array-type by enumerating all possible incorporation patterns leading to the array-type (i.e. an array of length 2 during a 3 day temporal input pattern could result from expansion on days {1,2}, {2,3}, or {1,3}) and then analytically calculated the sum of the probabilities of each incorporation pattern. This value was treated as the “global” array-type probability. After all array-type probabilities were calculated, the “global” probabilities for all array-types of a particular length were normalized to unity, resulting in the final predicted array-type frequency vector.

As an example of the model, for a single day of induction (state =1), the probability of an array containing an expanded spacer derived from pTrig (i.e. L1 array, T) is simply $p_{exp,1} * p_{T,1}^{L1}$. For one day of induction followed by one day of no induction (state = 10) the probability of an array containing two expanded spacers derived from pTrig (i.e. L2 array, TT) is simply $(p_{exp,1} * p_{T,1}^{L2}) * (p_{exp,0} * p_{T,0})$. For three days of induction (state = 111) the probability of an array containing two expanded spacers, one derived from the genome and the next derived from pTrig (i.e. L2 array, RT) is the sum of all incorporation patterns leading to RT arrays (incorporation on days {1,2}, {2,3}, {1,3}) or:

$$\begin{aligned}
 & [p_{exp,1} * (1 - p_{T,1}^{L2})] * (p_{exp,1} * p_{T,1}^{L2}) * (1 - p_{exp,1}) + \\
 & (1 - p_{exp,1}) * [p_{exp,1} * (1 - p_{T,1}^{L2})] * (p_{exp,1} * p_{T,1}^{L2}) + \\
 & [p_{exp,1} * (1 - p_{T,1}^{L2})] * (1 - p_{exp,1}) * (p_{exp,1} * p_{T,1}^{L2})
 \end{aligned}$$

Array type frequencies can be calculated for any input profile and array-type in a similar manner.

We used the array-type frequencies calculated from the model to classify the observed data. The Euclidean distance between observed array-type frequencies and predicted array-type frequencies was calculated, and the model with minimum distance to the observed data was selected as the predicted temporal input. This procedure can be repeated for different array lengths. To consider multiple array lengths simultaneously, aggregate array-type vectors were constructed by concatenating array-type vectors of different array lengths of interest (both observed and model) and the same procedure was used to calculate distance and predict temporal inputs.

Population lineage reconstruction using CRISPR array information

To perform lineage reconstruction, we identified genomic spacers within L1 arrays for the 16 4-day temporal recording samples (pooled from enriched and unenriched samples). Genomic spacers were utilized as they contain the highest sequence diversity, and L1 arrays were utilized given that they were observed with the highest frequencies in populations. These spacers were randomly subsampled for each sample to the minimum number of spacers detected (14,715). The location that each spacer mapped to on the reference genome was utilized as the identity of the spacer; the Jaccard distance between two samples (i.e. 1 – proportion of unique spacers in a sample shared with another sample) was calculated for all samples in a pairwise fashion. This 16x16 distance matrix was then utilized for lineage reconstruction using the Fitch-Margoliash method (42). Specifically, an tool implementing the PHYLIP program was utilized with default settings (<http://www.trex.uqam.ca/index.php?action=phylip&app=fitch>).

Multiplexed recording analysis and reconstruction

For all multiplexed temporal recordings, the full length DR sequence was utilized to enable differentiation of DR sequences. Given the strict criteria for DR matching utilized (no more than Hamming distance 2), this allowed for extraction of individual sensors from the CRISPR array populations.

Models were parameterized for each of the three sensors independently. Expansion rates in the absence and presence of signal ($p_{exp,0}$ and $p_{exp,1}$) were calculated as the average proportion of singly expanded arrays after 1 day for no input and input of all three chemicals (C,T,F) and the same value was utilized for all three sensors. pTrig incorporation rates in the absence of input ($p_{T,0}$) were calculated for each sensor from profile #1 (i.e. no input throughout the recording) as the average of pTrig spacers at all positions within L1 to L3 arrays. pTrig incorporation rates in the presence of input ($p_{T,1}^{L2}$, $p_{T,1}^{L3}$) were calculated for each sensor in a similar manner from profile #2 for L2 and L3 arrays separately. For the CopA sensor, we observed that pTrig spacer incorporation was higher when other inducers (T, F) were both present compared to other conditions. Therefore, the pTrig incorporation rate in the presence of input was calculate from profile #6, where the copper was present for three days but other inducers varied. All parameters utilized can be found in table S5.

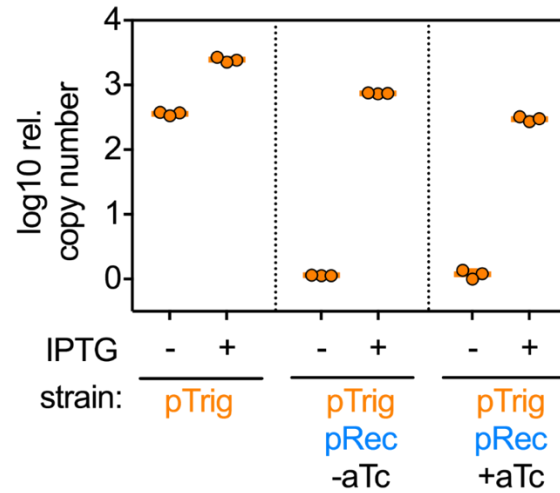


Fig. S1: pTrig copy number induction. To assess pTrig copy number increase in the context of recording, we measured pTrig copy number by qPCR. Cells with only pTrig displayed high copy number in the absence of inducer and low fold increase in copy number, since only genomic expression of LacI was present to repress the Lac promoter upstream of RepL on pTrig. The addition of pRec (which expresses LacI) resulted in repression of copy number in the absence of inducer and high fold increase in copy number after induction. Addition of aTc slightly decreased pTrig copy number during induction, indicating that Cas1 and Cas2 expression may reduce the apparent copy number of pTrig, for example by degradation.

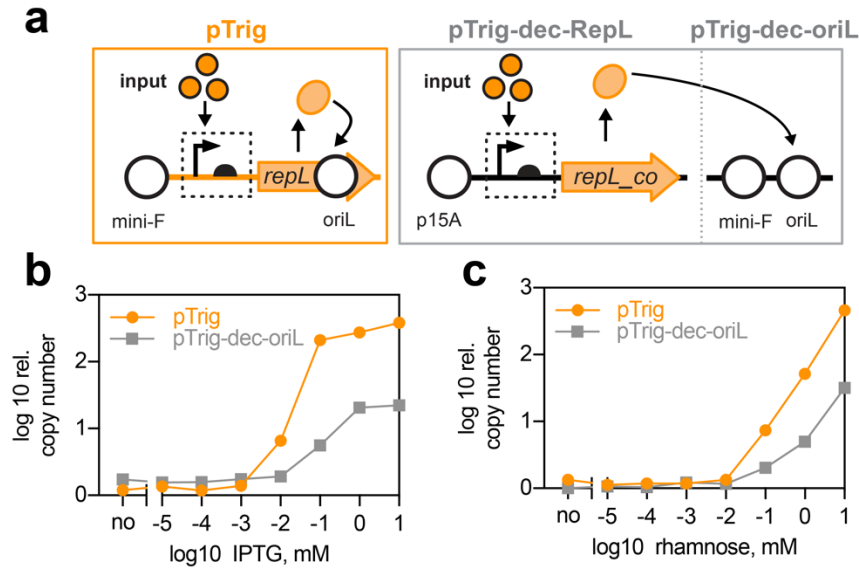


Fig. S2: Decoupling pTrig copy number induction. (a) To better understand the mechanism of pTrig copy number induction, RepL expression was decoupled from the amplifying effects of pTrig copy number increase. RepL was codon optimized for *E. coli* (to remove the origin of replication located within the RepL coding sequence) and placed on a p15A plasmid (pTrig-dec-RepL). The pTrig plasmid was then modified to remove the upstream promoter and first 100 bp of the RepL coding sequence, and a terminator (L3S1P52) was placed immediately upstream (to retain the RepL oriL origin of replication but eliminate expression; pTrig-dec-oriL). (b) The Lac promoter along with RiboJ and B0034 RBS was placed upstream of the RepL (pTrig-dec-RepL-Lac), and the decoupled system (pTrig-dec-RepL-Lac + pTrig-dec-oriL + pRec) was exposed to aTc and varying concentrations of IPTG for 6 hours alongside the pTrig system utilized in the main text. Plasmid copy number of pTrig or pTrig-dec-oriL was then measured by qPCR. The decoupled system displayed reduced range in copy induction and lower sensitivity to input compared to pTrig, suggesting that a positive feedback loop may mediate induction of the pTrig system. (c) To assess generality of the result, the experiment was repeated with a second inducible promoter. A rhamnose inducible promoter was swapped into the pTrig system (pTrig-Rha, 150 bp upstream sequence of *E. coli* RhaB, see also fig. S14). The same promoter with the addition of RiboJ and B0034 RBS was swapped into the RepL expression plasmid (pTrig-dec-RepL-Rha), and the decoupled system (pTrig-dec-RepL-Lac + pTrig-dec-oriL + pRec Δ LacI) was compared to the pTrig system (pTrig-Rha + pRec Δ LacI) as in (a) with aTc and varying concentrations of rhamnose inducer for 6 hours. A similar reduced copy number induction range and lower input sensitivity in the decoupled system compared to the pTrig system was also observed.

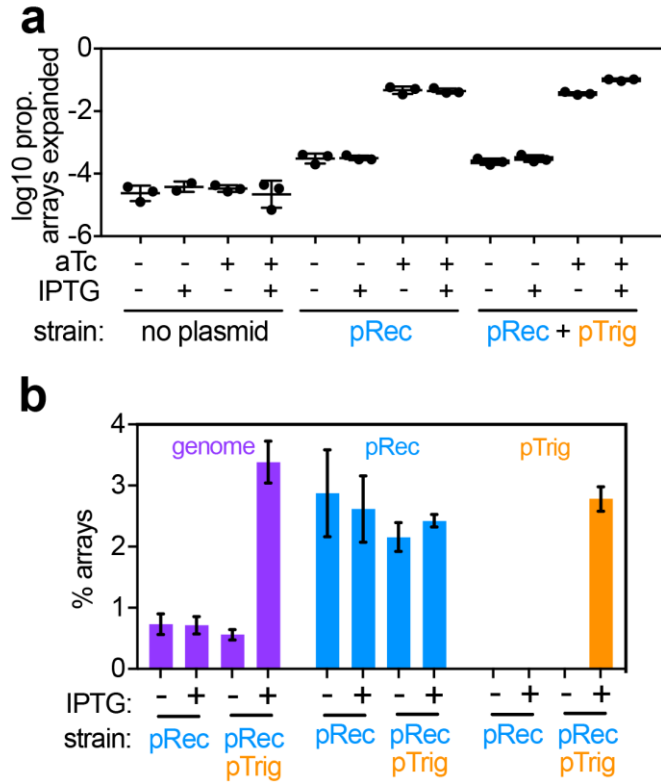


Fig. S3: CRISPR spacer acquisition. (a) CRISPR expansion, calculated as the log10 proportion of arrays detected as expanded, was assessed over the course of a single recording round. As a control, a strain harboring no plasmids was first tested. We detected a very low amount of expansion, presumably from index swapping between samples that can occur at background levels on the Illumina sequencing platform. For one of the no plasmid samples receiving only IPTG inducer, no expanded spacers were detected, therefore this replicate not plotted. Addition of pRec increased CRISPR expansion above background levels, likely due to leaky expression of Cas1 and Cas2; addition of aTc inducer greatly increased CRISPR expansion. The addition of pTrig did not affect CRISPR expansion without copy number induction by IPTG, but overall expansion increased when IPTG was added. (b) An alternative visualization of Fig. 1g. With the pTrig plasmid in the presence of IPTG, pTrig spacer acquisition greatly increases (other pTrig bars are not present as they are too small to be visualized on this Y-axis scale). pTrig induction did not appear to affect pRec spacer acquisition, but increased genomic spacer acquisition, indicating that pTrig copy number increase may interact with genomic replication or spacer acquisition processes. Error bars represent standard deviation of three biological replicates.

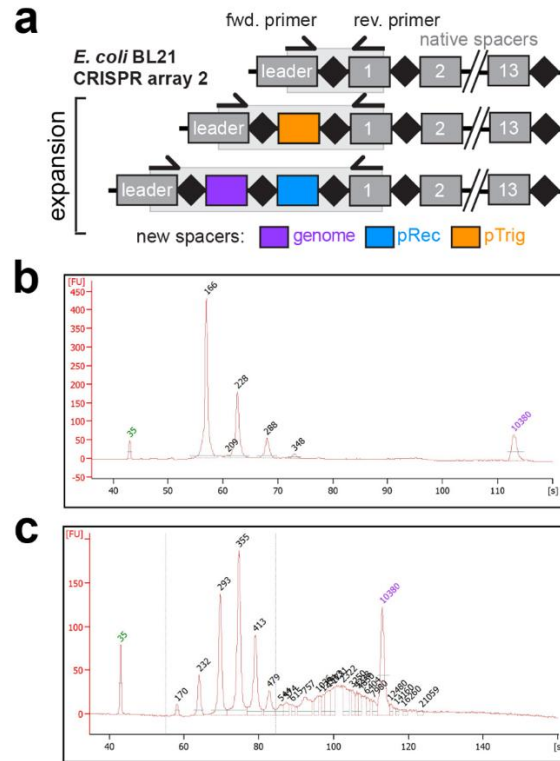


Fig. S4: CRISPR array sequencing. (a) Schematic of custom CRISPR amplicon sequencing approach. (b) Example library size distribution by Bioanalyzer HS DNA assay; the smallest product (~166 bp) corresponds to unexpanded arrays, and products of larger sizes, ~228, ~288, ~348 bp, correspond to expanded arrays of 1, 2, 3 spacers respectively. (c) Size-enriched library size distribution determined in the same manner as (b); expanded arrays are enriched. Contaminating high molecular weight DNA was observed (presumably plasmid or genomic DNA from the PCR template) but did not affect sequencing.

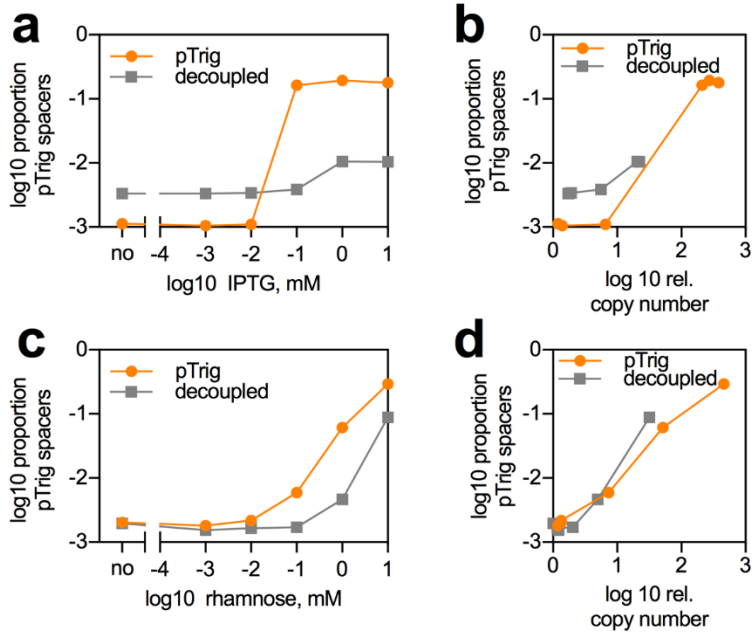


Fig. S5: Relationship between pTrig copy number and pTrig spacer incorporation. For the same experiment shown in fig. S2, cells were recovered and subjected to CRISPR array sequencing. **(a)** For the Lac pTrig and decoupled system, the resulting proportion of pTrig spacers is displayed in log₁₀ scale. **(b)** Spacer incorporation was directly compared to measured pTrig or pTrig-dec-oriL copy number (shown in fig. S2), and displayed an increasing relationship as expected. **(c,d)** The same data is shown for the Rha pTrig and decoupled system.

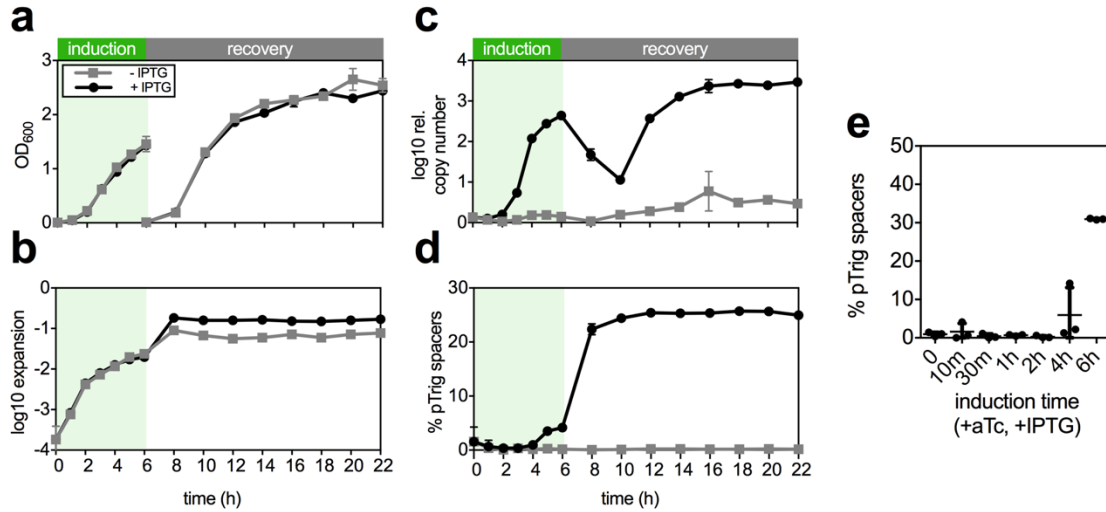


Fig. S6: CRISPR expansion and pTrig incorporation over a single induction round. We tracked culture growth, pTrig copy number and spacer acquisition over the course of induction and recovery to assess response dynamics of the system. Cells received aTc induction and were exposed to no IPTG or IPTG inducer; all points display the mean and standard deviation of three biological replicates. **(a)** Induction of pTrig did not appear to affect cell growth as measured by optical density compared to basal maintenance of the system. **(b)** Array expansion was observed after 1 hour of induction, and a large increase in spacer acquisition was observed during recovery. **(c)** pTrig copy number as measured by qPCR displayed an increase beginning 3 hours after induction. In addition, copy number increased during the recovery period only when cells had been previously induced, likely due to residual IPTG inducer in recovery media. Further dilution on the subsequent day prevents this re-activation from interfering with multi-day recordings. **(d)** The percentage of pTrig spacers appeared to increase after 4 hours, consistent with pTrig copy number dynamics. **(e)** The duration of induction (with aTc and IPTG) was varied between 0 to 6 hours and the recovery time was adjusted such that all samples were collected at the same time. Robust recording required the full 6 hours of induction.

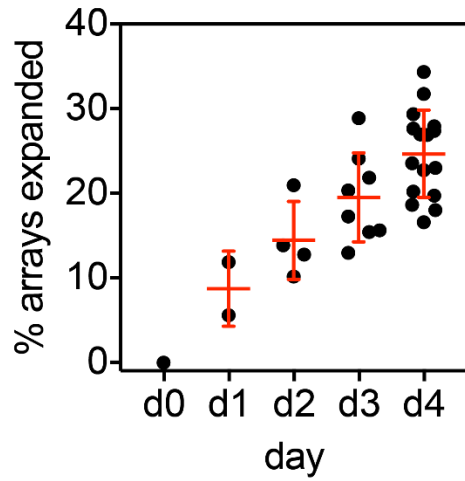


Fig. S7: CRISPR array expansion over multiple days. Samples from intermediate states (d1, d2, d3) were sequenced in addition to d4. The percent of CRISPR arrays detected as expanded in each sample is plotted; increasing array expansion was observed over the course of the experiment.

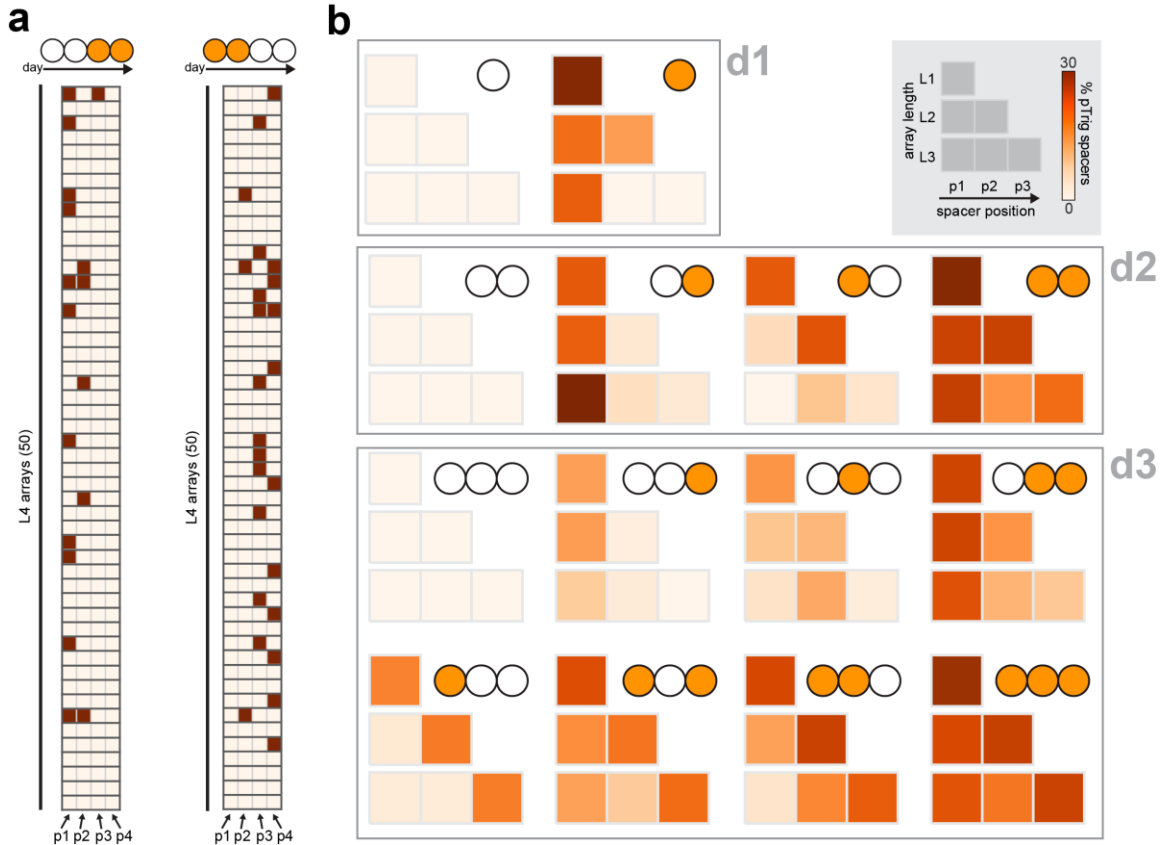


Fig. S8: pTrig spacer incorporation. (a) To visualize the information encoded within individual arrays, 50 L4 arrays sampled from two representative temporal input profiles are shown as a heatmap (as in Fig. 2d) where rows are individual arrays and columns are positions in the array (shaded: pTrig spacer, unshaded: reference spacer). The individual array information can be then visualized as positional averages as shown in the main text (Fig. 2e). (b) Samples from d1, d2 and d3 were additionally sequenced. The resulting %pTrig spacers detected for different array lengths (L1 to L3) at different positions (p1 to p3) is plotted as in Fig. 2e. L4 and L5 arrays are omitted as a low number were detected (intermediate samples were sequenced without the enrichment protocol).

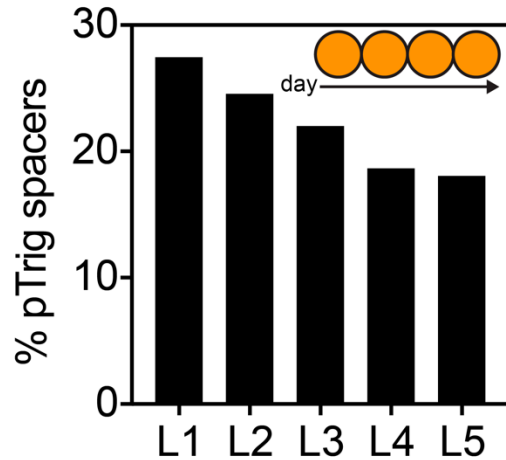


Fig. S9: CRISPR array length-dependence of pTrig incorporation for model parameterization. pTrig incorporation appeared to differ across different array lengths; for example the average percentage of pTrig spacers at each position of each array length for the sample receiving inducer for four days is shown. This is presumably due to the delayed activation of pTrig compared to array expansion; the first incorporations during a recording round are less likely to contain pTrig spacers as pTrig copy number has not yet increased. Therefore, highly expanded arrays may display slightly lower levels of pTrig incorporation. Given this trend, we individually parameterized models for each array-length by empirically using the average percentage of pTrig spacers found in each array length (i.e. using the values above, see table S5).

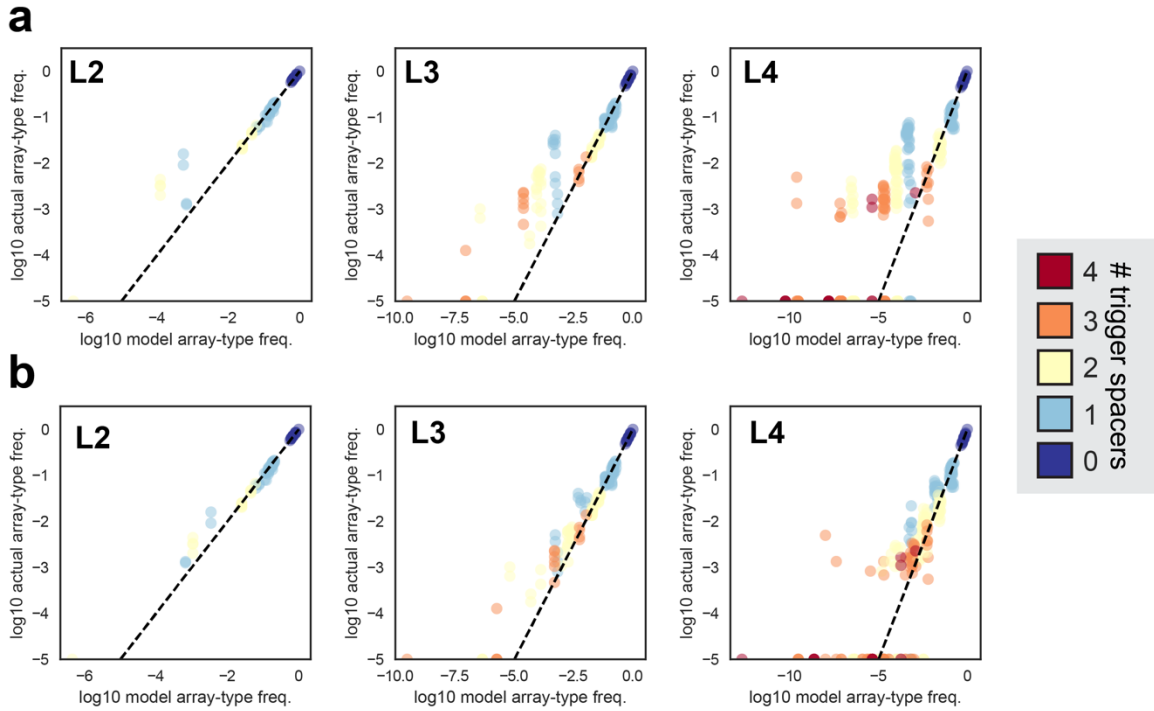


Fig. S10: Observed and predicted array-type frequencies for all four day input profiles. (a) The observed array-type frequencies from experimental data and modeled array-type frequencies are displayed for all 16 input profiles as an aggregate scatter plot, with both axes in log scale. The shading of each point indicates the number of trigger spacers the specific array-type contains. Array-types not observed in a particular sample are plotted on the X axis (i.e. log frequency = -5). Results for different array lengths are shown: L2 arrays, L3 arrays, L4 arrays. A close correspondence between the observed and predicted array-type frequencies is apparent, although a subset of low frequency array-types occur more often than predicted. (b) We hypothesized that the model assumption of only up to one expansion per day contributed to the discrepancy between data and model. We altered the model to allow a second expansion for singly expanded arrays at with the same probability as the first expansion but scaled by a constant value. This scaling factor (0.02402) was calculated as the proportion of doubly expanded arrays observed to singly expanded arrays observed from the same control experiment utilized to parameterize expansion rates. The same plots in (a) are shown for this two expansion model, and visually display better model recapitulation of low frequency array-types, suggesting better modeling of the CRISPR expansion process. For the sake of simplicity the single expansion model is still utilized for classification, but we note that more nuanced models of CRISPR expansion could allow for improved reconstruction performance.

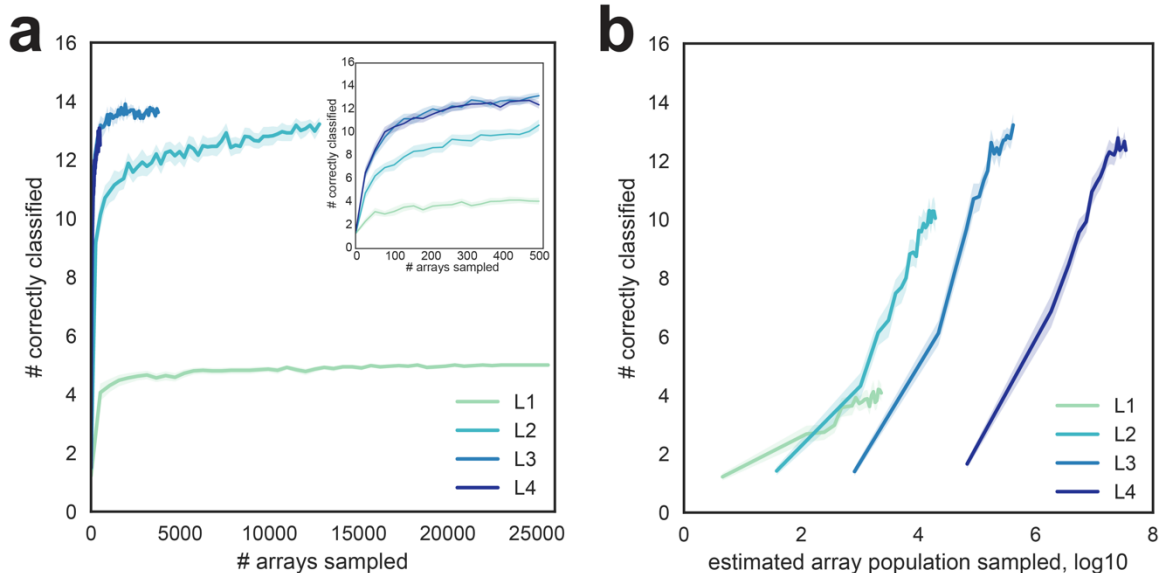


Fig. S11: Number of arrays required for classification of temporal input profiles. (a) For each of the 16 temporal profiles, arrays were subsampled to the minimum number detected for each array length (array lengths L1 to L4; decreasing arrays detected for increasing array lengths) and classification was performed. Lines display the mean and error bands display the 95% confidence interval of 50 iterations of subsampling and classification. In the inset, arrays are subsampled to 508 arrays (the minimum number arrays detected in any sample of any array length). These results demonstrate that only a few hundred arrays of a given length are required for reasonable classification performance. **(b)** The same subsampling and classification accuracy analysis was replotted with an estimate of the total array population required (log₁₀ scale), rather than the number of arrays of a given length as in (a). Specifically, the x-axis was rescaled utilizing the average proportion of arrays of a given length (L1 to L4) observed across the 16 temporal profile samples sequenced without size enrichment (Fig. 2b, dotted lines). These results demonstrate that a population of $\sim 10^5$ arrays (using L3 arrays for classification) can recapitulate reasonable accuracy ($\sim 75\%$ or 12/16 correctly classified).

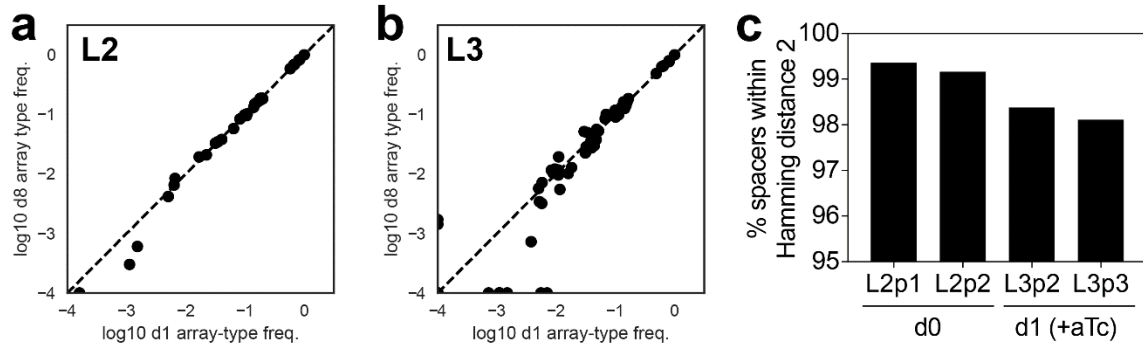


Fig. S12: Stability of TRACE recordings. Cell populations were subjected to 3 day temporal recording, resulting in 8 temporal profiles. The 8 populations were subsequently diluted 1:100 every 24 hours into 3mL fresh LB media with antibiotics for a total of 8 days (~6.6 generations per day, ~50 total generations). Array-type frequencies at d1 and d8 were then compared for all of the 8 profiles in aggregate for (a) array length 2 (L2) (b) and L3 arrays. Array types not detected in a sample are plotted on the axis (i.e. log frequency = -4). Array type frequencies appeared stable over the course of the experiment, although some low frequency array types exhibited variability likely due to population fluctuations. (c) A strain containing an array with two expanded spacers was clonally isolated, and induced with aTc with the same induction protocol utilized for recording. The strain before induction (d0) and after induction (d1) was sequenced. The percentage of extracted L2 spacer sequences within Hamming distance 2 of the actual expected sequence at d0 is displayed and was >99% at each position; other spacers likely represent sequencing errors or background levels of spacer loss. After induction, L3 arrays (i.e. arrays receiving a new spacer) were analyzed; the distal p2 and p3 positions largely contained the expected spacers with a small but measureable loss (~1%) compared to the background rate before induction. In sum, these experiments demonstrate stability of array type frequencies and thus recorded information, and a low rate of loss of previously recorded spacers.

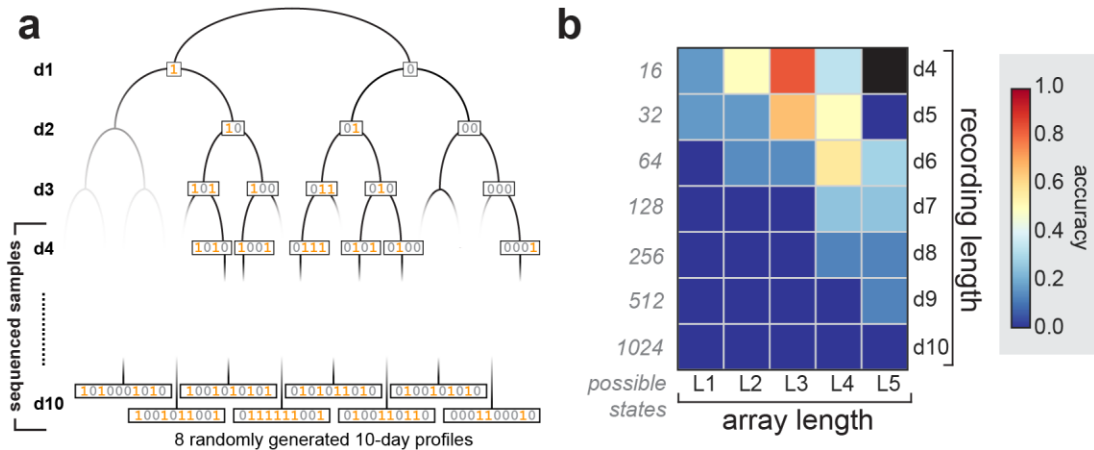


Fig. S13: 10-day temporal recording. A 10 day recording (~150 generations, ~15 generations per day) was performed to assess the limits of long term recording. **(a)** We randomly selected 8 of the 1024 (2^{10}) possible 10-day temporal input profiles (bottom boxes) and experimentally exposed 8 corresponding lineages to these input profiles in a similar manner to the 4 day experiment, utilizing a branching lineage method. Samples were collected at each time point from d4 to d10 for sequencing; given that some of the early time point substrings were shared between samples, not all early days contained 8 distinct samples (minimum 6 samples each day). Here, input exposures are displayed as a binary string (1 indicates induction and 0 indicates no induction) for clarity. **(b)** The data was then classified against models of all potential profiles and for array lengths L1-L5. We could obtain reasonable reconstruction accuracies up to d6 (L4 arrays: 4/7 tested correct, 1/64 expected by random guessing). In addition, arrays with more spacers appeared to enable better classification of input profiles of longer duration.

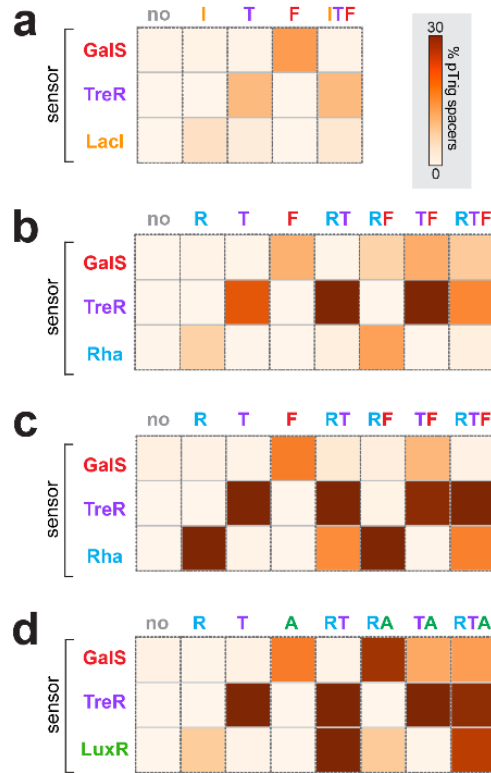


Fig. S14: Screening for orthogonal TRACE sensor systems. In preliminary experiments, we screened sensors and exposure conditions to identify three sensors displaying orthogonal function. In total, we demonstrated functionality of multi-channel sensing with six distinct sensing systems. **(a)** We first utilized the GalS and TreR sensor strains alongside the LacI sensor system. We found that each strain responded to its cognate inducer, however the GalS sensor displayed inactivation in the presence of IPTG and trehalose. A previous study has reported inactivation of the GalS sensor in response to IPTG, consistent with this result (43). **(b)** We constructed a rhamnose sensor, consisting of the 150 bp upstream sequence of *E. coli* RhaB swapped in place of the Lac promoter pTrig (pTrig-Rha); no transcription factor overexpression was utilized for this sensor system. This sensor was tested alongside the GalS and TreR sensor strains containing barcoded DR sequences. Populations of cells were exposed to combinatorial inputs (as in the main text; 1 mM rhamnose [R] was used as inducer for the Rha sensor). Again, we observed cognate response of each sensor to its ligand; however, we observed inactivation of the Rha sensor in the presence of trehalose. **(c)** We repeated the experiment in (b), but utilized 10 mM rhamnose rather than 1 mM rhamnose in an attempt to avoid trehalose inactivation of the Rha sensor strain. However, with these inducer conditions, we observed inactivation of the GalS sensor in the presence of rhamnose. These results highlight the complex interplay of endogenous sensing systems in *E. coli*, likely reflecting host sugar utilization hierarchies. **(d)** Finally, we constructed a 3OC6-HSL (i.e. AHL) sensor by swapping the D49 promoter (44) in place of the Lac promoter (pTrig-D49) and expressing the LuxR transcription factor on a variant of the pRec plasmid (pRec-LuxR). Populations of cells were exposed to combinatorial inputs (as in the main text; 100nM 3OC6-HSL [A] was used as inducer for the LuxR sensor). Each sensor displayed a response only to its cognate input.

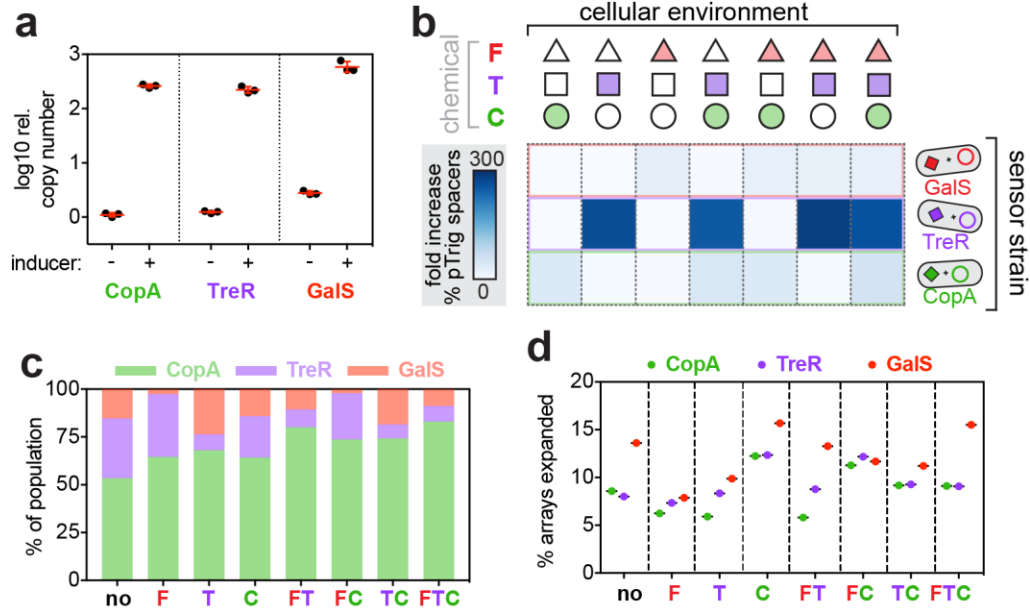


Fig. S15: Multi-channel recording with the TRACE system. (a) pTrig copy number characterization by qPCR for each of the three sensing systems individually exposed to their cognate input for 6 hours. (b) Fold increase (linear scale) in the percentage of pTrig spacers after recording for 7 input conditions compared to no inducer; all systems display >24 fold increase (each value displays the average of three biological replicates). The TreR sensor displays a higher fold increase compared to the two other systems. (c) The frequency of each of the three barcoded CRISPR arrays after the 8 inducer input exposures. All sensors are detected in each of conditions although with differing frequencies, suggesting that subtle fitness differences between sensor strains and during pTrig activation may result in altered population abundances. (d) The percentage of expanded arrays detected for each of the three sensors; the two barcoded arrays (TreR and GalS sensors) display similar expansion to the wild type array (CopA). This demonstrates that the barcoding does not impede the CRISPR expansion process for the two barcode sequences tested.

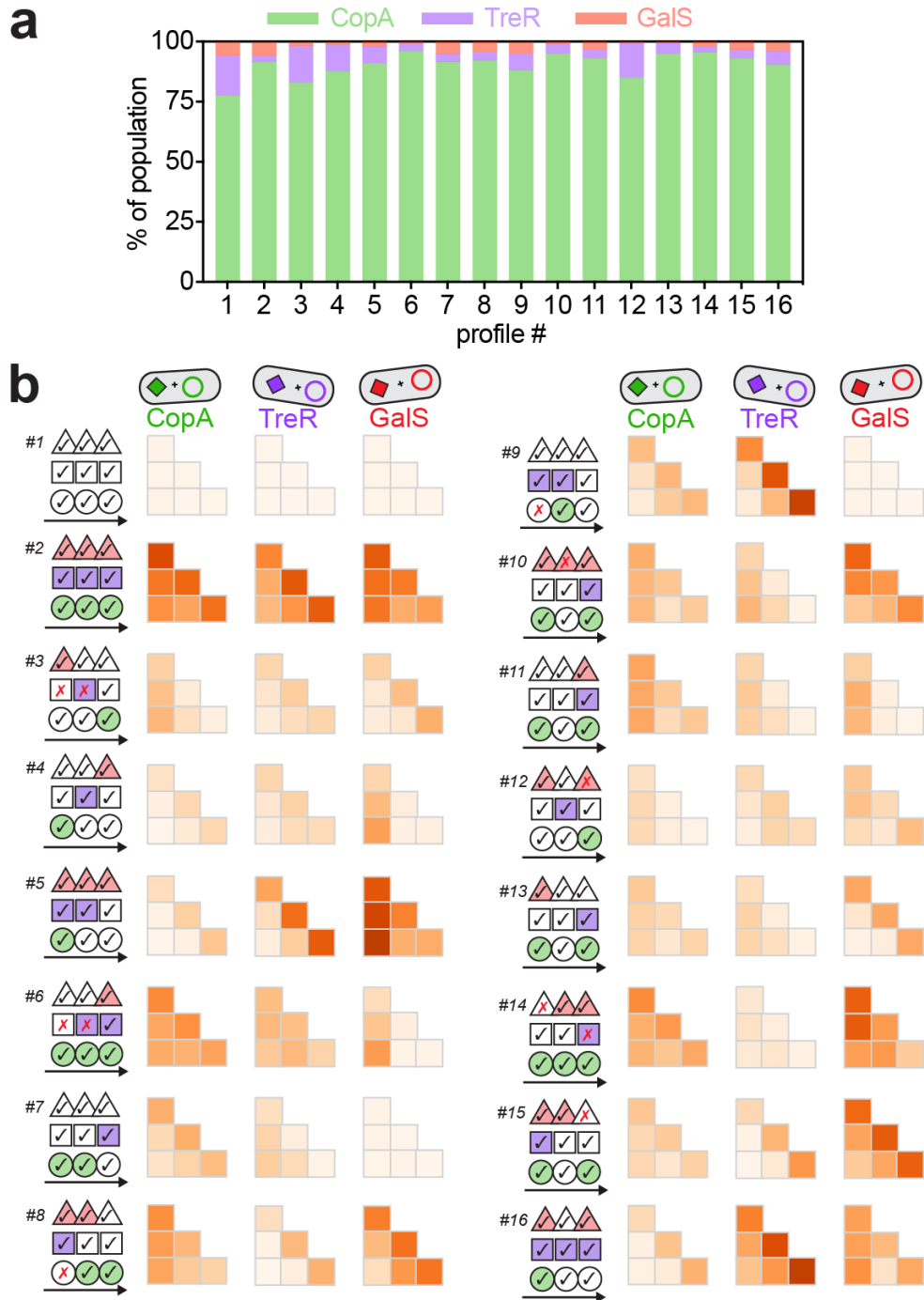


Fig. S16: Population frequencies and pTrig spacer incorporation for the multiplex temporal recording experiment. (a) The final frequency of each of the three barcoded CRISPR arrays at d3 is displayed for all 16 temporal profiles tested; frequencies vary per profile and sensor but all three are detected in each sample at a frequency of at least ~0.4%. **(b)** Average pTrig spacer incorporation for different array lengths (L1 to L3) and positions (p1 to p3) plotted as in Fig. 2e. To aid visualization, the color map for the CopA sensor ranges from 0 to 8%, while the color map for the TreR and GalS sensors ranges from 0 to 30%.

Table S1. Plasmids used in this study.

ref name	plasmid	resistance marker	origin	description
pRS001	pRec	CmR	ColE1	PTet-cas12, tetR, lacI
pRS002	pRec-GalS	CmR	ColE1	PTet-cas12, tetR, lacI-galS
pRS003	pRec-TreR	CmR	ColE1	PTet-cas12, tetR, lacI-treR
pRS004	pRec Δ LacI	CmR	ColE1	PTet-cas12, tetR
pRS005	pTrig	KanR	mini-F	PLac-repL
pRS006	pTrig-CopA	KanR	mini-F	PCopA-RiboJ-B0034-repL

ref name	plasmid	map
pRS001	pRec	https://benchling.com/s/seq-A9McFCX7BXXXI9vSBrRe
pRS002	pRec-GalS	https://benchling.com/s/seq-I8zistPSzTIXMneP5V4h
pRS003	pRec-TreR	https://benchling.com/s/seq-30jc7WJzBGX8fNKZp7Pz
pRS004	pRec Δ LacI	https://benchling.com/s/seq-cv8by55ejdFb4xCZD4d1
pRS005	pTrig	https://benchling.com/s/seq-ISWVXtHWPPuY5zCBNceM
pRS006	pTrig-CopA	https://benchling.com/s/seq-JBz03HXz2h1sDNJ4ob9P

Table S2. Strains used in this study.

strain	plasmid1	plasmid2
BL21		
BL21	pRec	
BL21	pRec	pTrig
BL21	pRec Δ LacI	pTrig-CopA
BL21 LacI_tKO DR_mut_1	pRec-TreR	pTrig
BL21 LacI_tKO DR_mut_2	pRec-GalS	pTrig

Table S3. Primers used in this study.

Primer	sequence (5'-3')
MAGE_tKO_LacI	G*G*A*A*GAGAGTCAATTCAGGGTGGTGAATGTGAAACCAGTA TAGT <u>GATAAGAT</u> GT <u>CGCAGAGT</u> ATGCCGGTGTCTCTTATCAGACCGTTTC
MAGE_BL21_DR	G*G*G*GAACACCCGTAAGTGGTTTGAGCGATGATATTTGTGCT NNNNNNNNCCCGCTGGCGCGGGGAACACTCTAAACATAACCTATTATT
genome_fwd	GCGAGCGATCCAGAAGATCT
genome_rev	GGGTAAAGGATGCCACAGACA
pTrig_fwd	CGCTCTATGATCCAGTCGATTT
pTrig_rev	TCCGTATGCCATGCGTTTAT

For the MAGE_tKO_LacI primer, underlined bases indicate mismatch with genomic LacI sequence. For the MAGE_BL21_DR primer, underlined bases indicate mismatch with genomic sequence designed to barcode individual arrays (note the last N base erroneously targets the first base pair of the first genomic spacer in the array). * indicates that the base immediately preceding symbol is phosphorothioated.

Table S4. CRISPR array sequencing primers.

primer	sequence (5'-3')
CB501	AATGATACGGCGACCACCGAGATCTACAC <u>TAGATCGC</u> ctggcttaaaaaatcattaattaataataggttatgtttaga
CB502	AATGATACGGCGACCACCGAGATCTACAC <u>CTCTCTAT</u> ctggcttaaaaaatcattaattaataataggttatgtttaga
CB503	AATGATACGGCGACCACCGAGATCTACAC <u>TATCCTCT</u> ctggcttaaaaaatcattaattaataataggttatgtttaga
CB504	AATGATACGGCGACCACCGAGATCTACAC <u>AGAGTAGA</u> ctggcttaaaaaatcattaattaataataggttatgtttaga
CB505	AATGATACGGCGACCACCGAGATCTACAC <u>GTAAGGAG</u> ctggcttaaaaaatcattaattaataataggttatgtttaga
CB506	AATGATACGGCGACCACCGAGATCTACAC <u>ACTGCATA</u> ctggcttaaaaaatcattaattaataataggttatgtttaga
CB507	AATGATACGGCGACCACCGAGATCTACAC <u>AAGGAGTA</u> ctggcttaaaaaatcattaattaataataggttatgtttaga
CB508	AATGATACGGCGACCACCGAGATCTACAC <u>CTAAGCCT</u> ctggcttaaaaaatcattaattaataataggttatgtttaga
CB701	CAAGCAGAAGACGGCATAACGAGAT <u>TCGCCTTA</u> ggtttgagcgatgatatttgctgct
CB702	CAAGCAGAAGACGGCATAACGAGAT <u>CTAGTACG</u> ggtttgagcgatgatatttgctgct
CB703	CAAGCAGAAGACGGCATAACGAGAT <u>TTCTGCCT</u> ggtttgagcgatgatatttgctgct
CB704	CAAGCAGAAGACGGCATAACGAGAT <u>GCTCAGGA</u> ggtttgagcgatgatatttgctgct
CB705	CAAGCAGAAGACGGCATAACGAGAT <u>AGGAGTCC</u> ggtttgagcgatgatatttgctgct
CB706	CAAGCAGAAGACGGCATAACGAGAT <u>CATGCCTA</u> ggtttgagcgatgatatttgctgct
CB707	CAAGCAGAAGACGGCATAACGAGAT <u>GTAGAGAG</u> ggtttgagcgatgatatttgctgct
CB708	CAAGCAGAAGACGGCATAACGAGAT <u>CCTCTCTG</u> ggtttgagcgatgatatttgctgct
CB709	CAAGCAGAAGACGGCATAACGAGAT <u>AGCGTAGC</u> ggtttgagcgatgatatttgctgct
CB710	CAAGCAGAAGACGGCATAACGAGAT <u>CAGCCTCG</u> ggtttgagcgatgatatttgctgct
CB711	CAAGCAGAAGACGGCATAACGAGAT <u>TGCTCTTT</u> ggtttgagcgatgatatttgctgct
CB712	CAAGCAGAAGACGGCATAACGAGAT <u>TCCTCTAC</u> ggtttgagcgatgatatttgctgct
CBR1	CTGGCTTAAAAAATCATTAATTAATAATAGGTTATGTTTAGAGTGTTCCTCCGCGCCAG
CBI1	CGGGGATAAACCGAGCACAAATATCATCGCTCAAACC

For all samples, underlined bases indicate barcode sequence (derived from Illumina Nextera barcodes).

Table S5: Parameters utilized in CRISPR expansion models

sensor	state	parameter	value	calculated from?
LacI	1	p_T, L1	0.27490	"1111" sample, pTrig proportion in L1 arrays
LacI	1	p_T, L2	0.24570	"1111" sample, average of pTrig proportion in L2 arrays
LacI	1	p_T, L3	0.22020	"1111" sample, average of pTrig proportion in L3 arrays
LacI	1	p_T, L4	0.18650	"1111" sample, average of pTrig proportion in L4 arrays
LacI	1	p_T, L5	0.18090	"1111" sample, average of pTrig proportion in L5 arrays
LacI	0	p_T	0.00070	"0000" sample, average of pTrig proportion at all positions (L1-L5)
LacI	1	p_exp	0.09880	average proportion singly expanded after single round (control experiment)
LacI	0	p_exp	0.03560	average proportion singly expanded after single round (control experiment)
CopA	1	p_T, L2	0.03542	profile #6, average of pTrig proportion in CopA sensor in L2 arrays
CopA	1	p_T, L3	0.03092	profile #6, average of pTrig proportion in CopA sensor in L3 arrays
CopA	0	P_T	0.00107	profile #1, average of pTrig proportion in CopA sensor at all array positions L1-L3
TreR	1	p_T, L2	0.16064	profile #2, average of pTrig proportion in TreR sensor in L2 arrays
TreR	1	p_T, L3	0.14790	profile #2, average of pTrig proportion in TreR sensor in L3 arrays
TreR	0	p_T	0.00065	profile #1, average of pTrig proportion in TreR sensor at all array positions L1-L3
GalS	1	p_T, L2	0.17542	profile #2, average of pTrig proportion in GalS sensor in L2 arrays
GalS	1	p_T, L3	0.13966	profile #2, average of pTrig proportion in GalS sensor in L3 arrays
GalS	0	p_T	0.00306	profile #1, average of pTrig proportion in GalS sensor at all array positions L1-L3
CopA/TreR/GalS	1	p_exp	0.10155	average proportion singly expanded after one day (across all sensors) with no inducer
CopA/TreR/GalS	0	p_exp	0.09829	average proportion singly expanded after one day (across all sensors) with all three inducers

References and Notes

1. A. E. Friedland, T. K. Lu, X. Wang, D. Shi, G. Church, J. J. Collins, Synthetic gene networks that count. *Science* **324**, 1199–1202 (2009). [doi:10.1126/science.1172005](https://doi.org/10.1126/science.1172005) [Medline](#)
2. J. Bonnet, P. Yin, M. E. Ortiz, P. Subsoontorn, D. Endy, Amplifying genetic logic gates. *Science* **340**, 599–603 (2013). [doi:10.1126/science.1232758](https://doi.org/10.1126/science.1232758) [Medline](#)
3. L. Yang, A. A. K. Nielsen, J. Fernandez-Rodriguez, C. J. McClune, M. T. Laub, T. K. Lu, C. A. Voigt, Permanent genetic memory with >1-byte capacity. *Nat. Methods* **11**, 1261–1266 (2014). [doi:10.1038/nmeth.3147](https://doi.org/10.1038/nmeth.3147) [Medline](#)
4. V. Hsiao, Y. Hori, P. W. Rothmund, R. M. Murray, A population-based temporal logic gate for timing and recording chemical events. *Mol. Syst. Biol.* **12**, 869–14 (2016). [doi:10.15252/msb.20156663](https://doi.org/10.15252/msb.20156663) [Medline](#)
5. N. Roquet, A. P. Soleimany, A. C. Ferris, S. Aaronson, T. K. Lu, Synthetic recombinase-based state machines in living cells. *Science* **353**, aad8559 (2016). [doi:10.1126/science.aad8559](https://doi.org/10.1126/science.aad8559) [Medline](#)
6. W. Pei, T. B. Feyerabend, J. Rössler, X. Wang, D. Postrach, K. Busch, I. Rode, K. Klapproth, N. Dietlein, C. Quedenau, W. Chen, S. Sauer, S. Wolf, T. Höfer, H.-R. Rodewald, Polylox barcoding reveals haematopoietic stem cell fates realized in vivo. *Nature* **548**, 456–460 (2017). [doi:10.1038/nature23653](https://doi.org/10.1038/nature23653) [Medline](#)
7. F. Farzadfard, T. K. Lu, Genomically encoded analog memory with precise in vivo DNA writing in living cell populations. *Science* **346**, 1256272 (2014). [doi:10.1126/science.1256272](https://doi.org/10.1126/science.1256272) [Medline](#)
8. A. McKenna, G. M. Findlay, J. A. Gagnon, M. S. Horwitz, A. F. Schier, J. Shendure, Whole-organism lineage tracing by combinatorial and cumulative genome editing. *Science* **353**, aaf7907 (2016). [doi:10.1126/science.aaf7907](https://doi.org/10.1126/science.aaf7907) [Medline](#)
9. K. L. Frieda, J. M. Linton, S. Hormoz, J. Choi, K. K. Chow, Z. S. Singer, M. W. Budde, M. B. Elowitz, L. Cai, Synthetic recording and in situ readout of lineage information in single cells. *Nature* **541**, 107–111 (2017). [doi:10.1038/nature20777](https://doi.org/10.1038/nature20777) [Medline](#)
10. S. T. Schmidt, S. M. Zimmerman, J. Wang, S. K. Kim, S. R. Quake, Quantitative analysis of synthetic cell lineage tracing using nuclease barcoding. *ACS Synth. Biol.* **6**, 936–942 (2017). [doi:10.1021/acssynbio.6b00309](https://doi.org/10.1021/acssynbio.6b00309) [Medline](#)
11. S. D. Perli, C. H. Cui, T. K. Lu, Continuous genetic recording with self-targeting CRISPR-Cas in human cells. *Science* **353**, aag0511 (2016). [doi:10.1126/science.aag0511](https://doi.org/10.1126/science.aag0511) [Medline](#)
12. R. Kalhor, P. Mali, G. M. Church, Rapidly evolving homing CRISPR barcodes. *Nat. Methods* **14**, 195–200 (2017). [doi:10.1038/nmeth.4108](https://doi.org/10.1038/nmeth.4108) [Medline](#)
13. S. A. Jackson, R. E. McKenzie, R. D. Fagerlund, S. N. Kieper, P. C. Fineran, S. J. J. Brouns, CRISPR-Cas: Adapting to change. *Science* **356**, eaal5056 (2017). [doi:10.1126/science.aal5056](https://doi.org/10.1126/science.aal5056) [Medline](#)
14. S. H. Sternberg, H. Richter, E. Charpentier, U. Qimron, Adaptation in CRISPR-Cas Systems. *Mol. Cell* **61**, 797–808 (2016). [doi:10.1016/j.molcel.2016.01.030](https://doi.org/10.1016/j.molcel.2016.01.030) [Medline](#)

15. A. V. Wright, J.-J. Liu, G. J. Knott, K. W. Doxzen, E. Nogales, J. A. Doudna, Structures of the CRISPR genome integration complex. *Science* **357**, 1113–1118 (2017). [doi:10.1126/science.aao0679](https://doi.org/10.1126/science.aao0679) [Medline](#)
16. R. Barrangou, C. Fremaux, H. Deveau, M. Richards, P. Boyaval, S. Moineau, D. A. Romero, P. Horvath, CRISPR provides acquired resistance against viruses in prokaryotes. *Science* **315**, 1709–1712 (2007). [doi:10.1126/science.1138140](https://doi.org/10.1126/science.1138140) [Medline](#)
17. J. McGinn, L. A. Marraffini, CRISPR-Cas systems optimize their immune response by specifying the site of spacer integration. *Mol. Cell* **64**, 616–623 (2016). [doi:10.1016/j.molcel.2016.08.038](https://doi.org/10.1016/j.molcel.2016.08.038) [Medline](#)
18. L. A. Marraffini, CRISPR-Cas immunity in prokaryotes. *Nature* **526**, 55–61 (2015). [doi:10.1038/nature15386](https://doi.org/10.1038/nature15386) [Medline](#)
19. S. L. Shipman, J. Nivala, J. D. Macklis, G. M. Church, Molecular recordings by directed CRISPR spacer acquisition. *Science* **353**, aaf1175 (2016). [doi:10.1126/science.aaf1175](https://doi.org/10.1126/science.aaf1175) [Medline](#)
20. S. L. Shipman, J. Nivala, J. D. Macklis, G. M. Church, CRISPR-Cas encoding of a digital movie into the genomes of a population of living bacteria. *Nature* **547**, 345–349 (2017). [doi:10.1038/nature23017](https://doi.org/10.1038/nature23017) [Medline](#)
21. A. Levy, M. G. Goren, I. Yosef, O. Auster, M. Manor, G. Amitai, R. Edgar, U. Qimron, R. Sorek, CRISPR adaptation biases explain preference for acquisition of foreign DNA. *Nature* **520**, 505–510 (2015). [doi:10.1038/nature14302](https://doi.org/10.1038/nature14302) [Medline](#)
22. M. B. Łobocka, D. J. Rose, G. Plunkett 3rd, M. Rusin, A. Samojedny, H. Lehnherr, M. B. Yarmolinsky, F. R. Blattner, Genome of bacteriophage P1. *J. Bacteriol.* **186**, 7032–7068 (2004). [doi:10.1128/JB.186.21.7032-7068.2004](https://doi.org/10.1128/JB.186.21.7032-7068.2004) [Medline](#)
23. I. Yosef, M. G. Goren, U. Qimron, Proteins and DNA elements essential for the CRISPR adaptation process in *Escherichia coli*. *Nucleic Acids Res.* **40**, 5569–5576 (2012). [doi:10.1093/nar/gks216](https://doi.org/10.1093/nar/gks216) [Medline](#)
24. J. K. Nuñez, L. Bai, L. B. Harrington, T. L. Hinder, J. A. Doudna, CRISPR immunological memory requires a host factor for specificity. *Mol. Cell* **62**, 824–833 (2016). [doi:10.1016/j.molcel.2016.04.027](https://doi.org/10.1016/j.molcel.2016.04.027) [Medline](#)
25. J. K. Nuñez, A. S. Y. Lee, A. Engelman, J. A. Doudna, Integrase-mediated spacer acquisition during CRISPR-Cas adaptive immunity. *Nature* **519**, 193–198 (2015). [doi:10.1038/nature14237](https://doi.org/10.1038/nature14237) [Medline](#)
26. H. H. Wang, F. J. Isaacs, P. A. Carr, Z. Z. Sun, G. Xu, C. R. Forest, G. M. Church, Programming cells by multiplex genome engineering and accelerated evolution. *Nature* **460**, 894–898 (2009). [doi:10.1038/nature08187](https://doi.org/10.1038/nature08187) [Medline](#)
27. J. M. Pickard, C. F. Maurice, M. A. Kinnebrew, M. C. Abt, D. Schenten, T. V. Golovkina, S. R. Bogatyrev, R. F. Ismagilov, E. G. Pamer, P. J. Turnbaugh, A. V. Chervonsky, Rapid fucosylation of intestinal epithelium sustains host-commensal symbiosis in sickness. *Nature* **514**, 638–641 (2014). [doi:10.1038/nature13823](https://doi.org/10.1038/nature13823) [Medline](#)

28. J. Elbaz, P. Yin, C. A. Voigt, Genetic encoding of DNA nanostructures and their self-assembly in living bacteria. *Nat. Commun.* **7**, 11179 (2016). [doi:10.1038/ncomms11179](https://doi.org/10.1038/ncomms11179) [Medline](#)
29. S. Silas, G. Mohr, D. J. Sidote, L. M. Markham, A. Sanchez-Amat, D. Bhaya, A. M. Lambowitz, A. Z. Fire, Direct CRISPR spacer acquisition from RNA by a natural reverse transcriptase-Cas1 fusion protein. *Science* **351**, aad4234 (2016). [doi:10.1126/science.aad4234](https://doi.org/10.1126/science.aad4234) [Medline](#)
30. R. Heler, A. V. Wright, M. Vucelja, D. Bikard, J. A. Doudna, L. A. Marraffini, Mutations in Cas9 enhance the rate of acquisition of viral spacer sequences during the CRISPR-Cas immune response. *Mol. Cell* **65**, 168–175 (2017). [doi:10.1016/j.molcel.2016.11.031](https://doi.org/10.1016/j.molcel.2016.11.031) [Medline](#)
31. C. Engler, R. Kandzia, S. Marillonnet, A one pot, one step, precision cloning method with high throughput capability. *PLOS ONE* **3**, e3647 (2008). [doi:10.1371/journal.pone.0003647](https://doi.org/10.1371/journal.pone.0003647) [Medline](#)
32. H. M. Salis, E. A. Mirsky, C. A. Voigt, Automated design of synthetic ribosome binding sites to control protein expression. *Nat. Biotechnol.* **27**, 946–950 (2009). [doi:10.1038/nbt.1568](https://doi.org/10.1038/nbt.1568) [Medline](#)
33. R. Lutz, H. Bujard, Independent and tight regulation of transcriptional units in *Escherichia coli* via the LacR/O, the TetR/O and AraC/I1-I2 regulatory elements. *Nucleic Acids Res.* **25**, 1203–1210 (1997). [doi:10.1093/nar/25.6.1203](https://doi.org/10.1093/nar/25.6.1203) [Medline](#)
34. C. Lou, B. Stanton, Y.-J. Chen, B. Munsky, C. A. Voigt, Ribozyme-based insulator parts buffer synthetic circuits from genetic context. *Nat. Biotechnol.* **30**, 1137–1142 (2012). [doi:10.1038/nbt.2401](https://doi.org/10.1038/nbt.2401) [Medline](#)
35. S. Meinhardt, M. W. Manley Jr., N. A. Becker, J. A. Hessman, L. J. Maher 3rd, L. Swint-Kruse, Novel insights from hybrid LacI/GalR proteins: Family-wide functional attributes and biologically significant variation in transcription repression. *Nucleic Acids Res.* **40**, 11139–11154 (2012). [doi:10.1093/nar/gks806](https://doi.org/10.1093/nar/gks806) [Medline](#)
36. M. T. Bonde, M. S. Klausen, M. V. Anderson, A. I. N. Wallin, H. H. Wang, M. O. A. Sommer, MODEST: A web-based design tool for oligonucleotide-mediated genome engineering and recombineering. *Nucleic Acids Res.* **42**, W408–W415 (2014). [doi:10.1093/nar/gku428](https://doi.org/10.1093/nar/gku428) [Medline](#)
37. K. A. Datsenko, B. L. Wanner, One-step inactivation of chromosomal genes in *Escherichia coli* K-12 using PCR products. *Proc. Natl. Acad. Sci. U.S.A.* **97**, 6640–6645 (2000). [doi:10.1073/pnas.120163297](https://doi.org/10.1073/pnas.120163297) [Medline](#)
38. S. J. Brouns, M. M. Jore, M. Lundgren, E. R. Westra, R. J. H. Slijkhuis, A. P. L. Snijders, M. J. Dickman, K. S. Makarova, E. V. Koonin, J. van der Oost, Small CRISPR RNAs guide antiviral defense in prokaryotes. *Science* **321**, 960–964 (2008). [doi:10.1126/science.1159689](https://doi.org/10.1126/science.1159689) [Medline](#)
39. M. Škulj, V. Okršlar, S. Jalen, S. Jevsevar, P. Slanc, B. Strukelj, V. Menart, Improved determination of plasmid copy number using quantitative real-time PCR for monitoring fermentation processes. *Microb. Cell Fact.* **7**, 6 (2008). [doi:10.1186/1475-2859-7-6](https://doi.org/10.1186/1475-2859-7-6) [Medline](#)

40. J. J. Kozich, S. L. Westcott, N. T. Baxter, S. K. Highlander, P. D. Schloss, Development of a dual-index sequencing strategy and curation pipeline for analyzing amplicon sequence data on the MiSeq Illumina sequencing platform. *Appl. Environ. Microbiol.* **79**, 5112–5120 (2013). [doi:10.1128/AEM.01043-13](https://doi.org/10.1128/AEM.01043-13) [Medline](#)
41. C. Camacho, G. Coulouris, V. Avagyan, N. Ma, J. Papadopoulos, K. Bealer, T. L. Madden, BLAST+: Architecture and applications. *BMC Bioinformatics* **10**, 421 (2009). [doi:10.1186/1471-2105-10-421](https://doi.org/10.1186/1471-2105-10-421) [Medline](#)
42. W. M. Fitch, E. Margoliash, Construction of phylogenetic trees. *Science* **155**, 279–284 (1967). [doi:10.1126/science.155.3760.279](https://doi.org/10.1126/science.155.3760.279) [Medline](#)
43. D. L. Shis, F. Hussain, S. Meinhardt, L. Swint-Kruse, M. R. Bennett, Modular, multi-input transcriptional logic gating with orthogonal LacI/GalR family chimeras. *ACS Synth. Biol.* **3**, 645–651 (2014). [doi:10.1021/sb500262f](https://doi.org/10.1021/sb500262f) [Medline](#)
44. R. S. Cox 3rd, M. G. Surette, M. B. Elowitz, Programming gene expression with combinatorial promoters. *Mol. Syst. Biol.* **3**, 145 (2007). [doi:10.1038/msb4100187](https://doi.org/10.1038/msb4100187) [Medline](#)